MIXING IN SMALL WARM CUMULI

H. Gerber*

Gerber Scientific, Inc., Reston, Virginia

ABSTRACT

High resolution (500 Hz data; 20-cm horizontal in-cloud) Re (droplet effective radius) and LWC (liquid water content) aircraft measurements made during RICO in trade-wind cumuli (Cu) are used to identify cloud parcels showing reduced Re values assumed to be caused by entrainment and droplet evaporation. Re are also calculated based on measured FSSP droplet size spectra exposed to hypothetical sub-saturated entrained air. Matches between measured and calculated values of Re give estimates of RH_e (relative humidity of the entrained air) in the form of pdfs and average values (~97%) at two levels above cloud base. Calculated time dependence of droplet evaporation at the high value of RH_e and other factors lead to the conclusion that mixing following entrainment is dominated by homogenous mixing rather than inhomogeneous mixing or inhomogeneous extreme mixing in the Cu that were analyzed here.

1. INTRODUCTION

The effective radius (Re) in warm cumulus clouds (Cu) without excessive precipitation is thought to be approximately constant with some reductions in Re observed occasionally (e.g., see Blyth and Latham, 1991.) This study again observes the variation of Re, this time in trade-wind Cu from the RICO (Rain in Cumulus over the Ocean) aircraft field study (Rauber et al., 2007.) The difference between the 1991 and the present study is the use of much higher in-cloud resolution for the Re and LWC measurements. Re and LWC data are collected with the PVM-100A probe (Gerber et al., 1994) at a maximum resolution of 10 cm along the flight path. This resolution is several orders of magnitude better than droplet size information obtained from droplet spectrometers, especially if the droplet concentration is low as in trade-wind Cu.

This study identifies the location of reduced values of Re thought to be caused by droplet evaporation associated with entrainment during aircraft passes through the Cu, quantifies the amount of Re reductions, and estimates the ambient RH_e (relative humidity) of the entrained air that causes the Re reductions. This information is used to estimate which of the three mixing processes between the entrained and cloud air (inhomogeneous extreme, inhomogenous, and homogeneous mixing; Baker and Latham, 1979; Baker et al., 1980) dominates the Cu. The mixing types are important because they affect differently droplet

microphysics and thus cloud lifetime, precipitation formation, and optics.

This is another mixing study for Cu given the lack of consensus on the nature of the mixing process as the following sample of findings shows: Jensen and Baker (1989) find droplet evaporation due to mixing is closer to homogeneous. Andrejczuk et al. (2006) find mixing to be neither totally homogeneous nor extreme inhomogeneous. Mixing is more inhomogeneous with increasing cloud life time (Schmeissner et al., 2015.) Small et al. (2013) and Jarecka et al. (2013) find homogeneous mixing increases with height in the Cu. Mixing is inhomogeneous (Beals et al., 2015.) Gerber et al. (2008) find inhomogeneous mixing increases with height. Homogeneous mixing is more likely in cloud cores, and inhomogenous mixing dominates diluted cloud (Lehmann et al., 2009). Activation of entrained CCN does not affect Cu microphysics and the mixing diagram (Small et al., 2013), while Gerber et al. (2008) and Schmeissner et al. (2015) find such an effect. Pinsky and Khain (2018) find that the mixing diagram is independent of ambient RH.

Here horizontal cloud passes are analyzed in low-precipitation Cu on flight RF12 from RICO described in Gerber et al. (2008). The passes have significant limitations in attempting to clarify the mixing process because the aircraft data is nearly instantaneous and thus without any time dependence of the mixing process as pointed out by Small et al. (2013) and Pinsky and Khain (2018) in their discussions of mixing diagrams. Therefore, the following analysis must contain assumptions. The following sections give instrumentation description, observational data, droplet evaporation, pdf of RH associated with entrainment, and conclusions.

---

*Corresponding author address: H. Gerber

Gerber Scientific, Inc., Reston, VA 20190

email: hgerber6@comcast.net

2. AIRCRAFT DATA

Probes on the NCAR C-130 aircraft collected data for flight RF12. Here some of the earlier analysis from Gerber et al. (2008) is used, and the analysis uses high-rate Re data from the PVM-100A aircraft probe. This probe measures simultaneously LWC (liquid water content; g m^{-3}) and PSA (particle area; cm^2 m^{-3}) in the same irradiated cloud volume at a rate of 1000 Hz corresponding to an in-cloud resolution of ~ 10 cm at the aircraft speed of ~100 m s^{-1}. The Re data used here are averaged to yield ~20-cm in-cloud resolution. Re = 30,000 x LWC/(ρ_w x PSA) where ρ_w is water density. Given that Re is proportional to LWC/PSA requires high accuracy when the denominator approaches zero value. Both outputs show some optical/electronic noise which is minimized by letting Re = 0 μm when PSA < 60 cm^2 m^{-3} and LWC < 0.002 g m^{-3}. The offsets in both channels is zeroed out when the PVM is out of cloud. The calibration of the PVM-100A is described in Gerber et al. (1994.) The accuracy of LWC measurements is 10% for r < 18 μm droplet radius, and the accuracy is 15% for 4 μm < Re < 12 μm; for both the accuracy decreases outside of those limits. The FSSP-100 droplet spectrometer probe is also used in this analysis. It produces 1-Hz droplet spectra (~100-m in-cloud resolution) over a size range of 0.35 μm to 22.83 μm droplet radius in 30 increments of 0.775 μm.

3. OBSERVATIONS

This analysis concentrates on five aircraft passes through each of two levels (250 m and 620 m) in growing Cu above the ocean surface on flight RF12. These two levels are part of five levels described in Gerber et al. (2008) for the same flight. One of the passes (#21) through a Cu at the ~620 m level is illustrated in Fig. 1 showing 20-cm resolution data of LWC and Re. The value of Re is remarkably steady in this plot, supporting such previous observations. It is not surprising that the few reduced Re values (red data points) from the steady background Re are near cloud edges given the proximity to dryer ambient air. The reductions occur over relatively small distances ranging from 0.2 m to 2 m in length; and the reductions are mostly missing in the rest of the Re data even in cloud segments with reduced values of LWC such as between ~100 m and ~200 m. Such behavior could be a result of 1) extreme inhomogeneous mixing thus preserving Re, 2) dilution of cloud with ambient air close to saturation, and 3) short mixing lifetimes of the reduced Re parcels because of their small size.
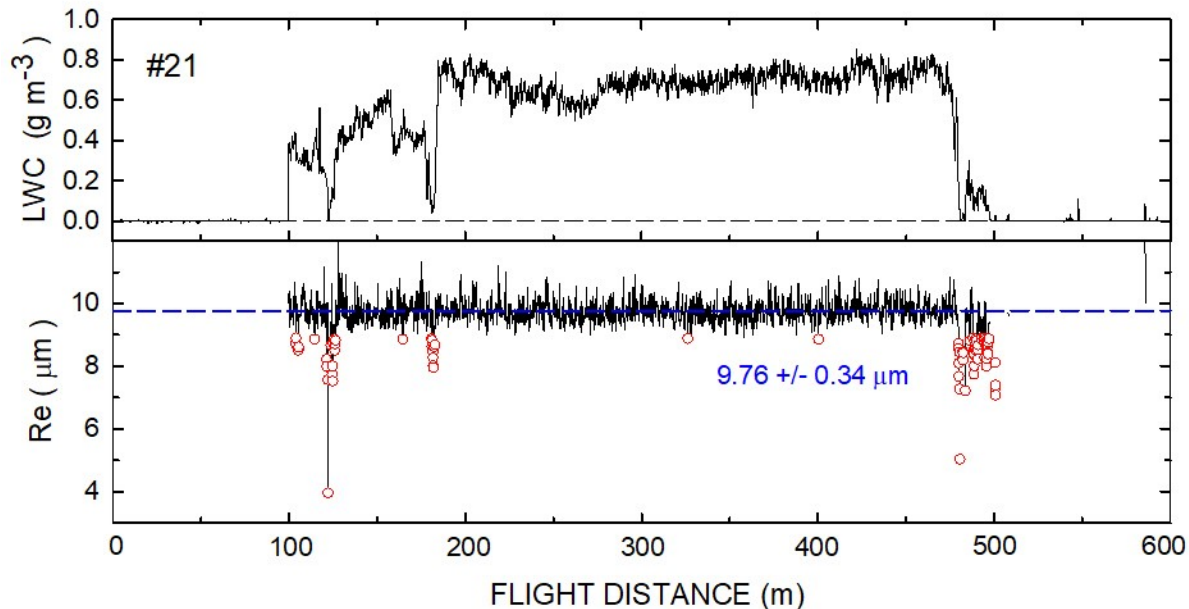

Fig. 1 – 20-cm resolution LWC and Re (effective radius) data in trade-wind Cu pass #21 on RICO flight RF12. Red data are Re values smaller than background Re and are assumed to be cloud parcels associated with entrainment, mixing, and droplet evaporation. Flight distance between 300 m and 400 m is the time interval (1 s) over which a FSSP droplet size spectrum was measured. The numerical Re is the average background Re +/- one std. dev. Data for Re ~ 0 μm are not included.

Figure 2 shows data from one of the passes (#6) through a growing Cu at the 250-m level. The 20-cm LWC and Re data for this pass look very different from the Fig. 1 data. Reductions of Re are again seen near the edges of the Cu (cloud at 50 m to 120 m is considered outside of the main cloud and is not analyzed.) However, a large section within the Cu shows reduced Re values which could be a result of entrainment of a larger eddy or overturning (toroidal circulation) which can occur in Cu (Blyth, 1993; Damiana et al., 2006.) Gerber et al. (2008) make the case that #6 illustrates the result of entrained and activated CCN (cloud condensation nuclei.) Averaging of the high-rate Re data would show substantial Re reductions as also observed occasionally by Blyth and Latham (1990).
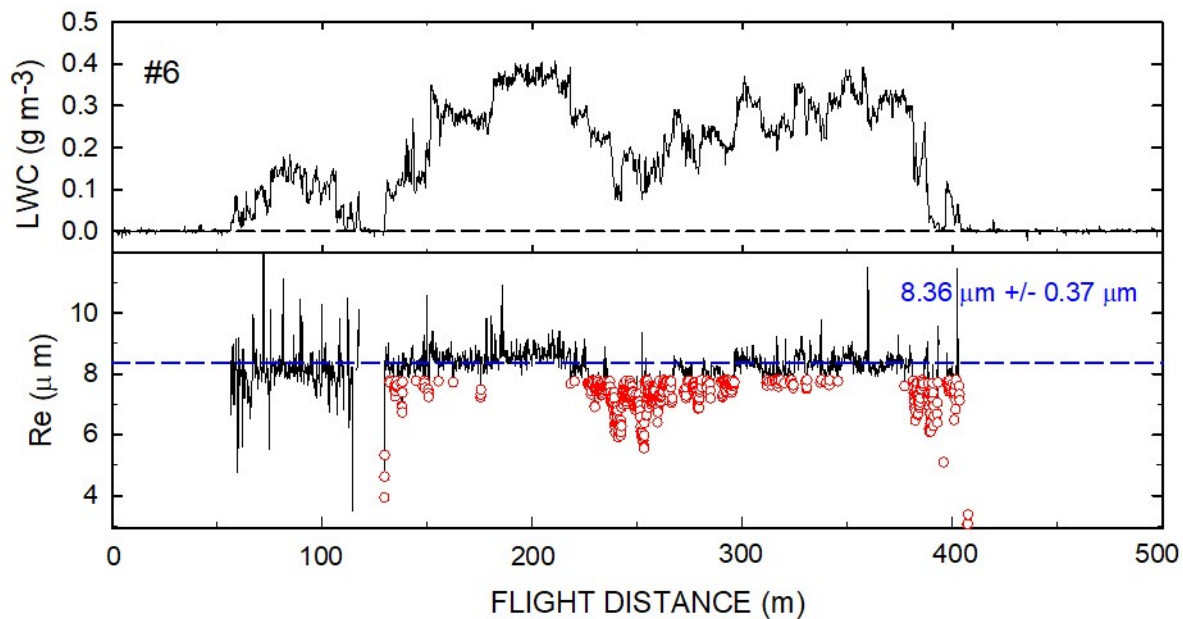

Fig. 2 – Same as Fig. 1, except for trade-wind Cu traverse #6 on RICO flight RF12.

The #6 and #21 cloud passes, as well as the other passes in the 35-cloud set described by (Gerber et al., 2008), provide new observational information from the high-rate PVM data: *In-cloud segments ("cloud holes") with LWC and Re ~ 0 um are exceptionally rare*, <0.4%, (except for the dissipating Cu at the highest level) even at the maximum PVM-100A resolution of 10 cm, suggesting that RH of the entrained air has high values limiting total evaporation of all droplets. Features such as shown for #6 occur occasionally in the growing Cu. The Re data often show significant slow-rate variability correlated with large LWC fluctuations suggesting prior droplet evaporation and mixing.

The amount of reduced Re for each red 20-cm resolution data point is the difference between the background Re and the reduced Re. These data are tabulated for the five passes at each of the two levels.

4. DROPLET EVAPORATION

4.1 Droplet spectral response

The response of the droplet spectrum measured for #21 is calculated as a function of hypothetical values of the entrained parcel's ambient RH. The goal is to produce a relationship between ambient RH and the reduced Re values in the spectrum. A match between the calculated and observed Re values then yields an estimate of the ambient RH associated with the entrainment mixing process. It is assumed that the #21 spectrum is typical of in-cloud spectra not affected recently by entrainment and that this spectrum mixes with entrained parcels near cloud edges for this Cu.

The calculations use the classical droplet growth equation $r\, dr/dt = C \times (S - S_e)$ (e.g., see Twomey, 1977) applied to the #21 spectrum under isobaric conditions. It is assumed that the entrained parcel and the cloud form a mixture instantaneously so that all droplets are exposed to the same sub-saturated value of relative humidity (RH_c). S is the supersaturation of the mixture, S_e is the equilibrium supersaturation at the surface of the droplets, and C contains the accommodation and condensation coefficients. S and RH_c are related by $S = (RH_c/100\%) -1.0$.

The measured #21 spectrum is shown in Fig. 3 (solid data points) along with spectra (hollow data points)

calculated by exposing the #21 spectrum to different values of $RH_c < 100\%$. The calculations require the mixing fraction χ which is the mass fraction of entrained air assumed to be 0.5. This value of χ dilutes by half the original droplet concentration N (135 cm^{-3}) of #21. Also needed is the time over which the growth equation is applied to obtain the calculated curves in Fig. 3. The chosen time of 15 s is 5-s larger than the mixing time scale (τ_{mix}; Baker et al. 1984) for #21 based on the average dissipation rate ($\varepsilon \sim 60$ cm^{2}s^{-3}) and entrained parcel dimension (~2 m) given in Gerber et al. (2008.) Over this time interval the entrained mixture is assumed to be lost by mixing with the rest of the cloud. A time step of 0.2 s is used in integrating the growth equation. The value of S is adjusted at each step to take into account cooling and water vapor produced by droplet evaporation.
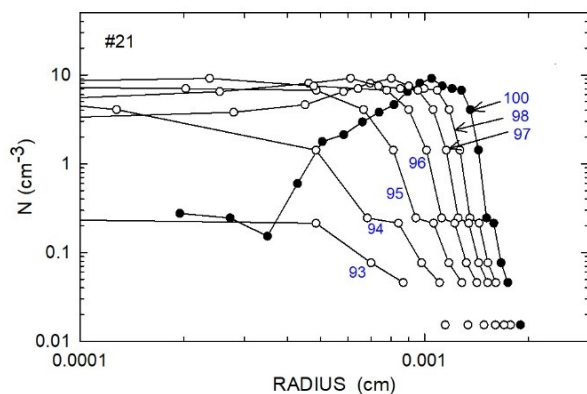

Fig. 3 – The droplet size distribution (solid data points) measured by the FSSP probe over the 1-s interval described in Fig. 1 for aircraft pass #21. Hollow data points are the response over 15 s of the original size distribution after it has been exposed instantaneously to various sub-saturated values of relative humidity RH_c of the entrained parcel and cloud mixture. The droplet number concentration N is given for each size bin of the FSSP probe. Each bin is 0.775 μm wide.

The value of Re is derived from each calculated spectrum for droplet radii between 2 μm and 25 μm in Fig. 3 and is shown as a function of RH_c in Fig. 4 for #21 (squares data.) The same procedure is done for the other passes at the two levels in Fig. 4. The data for #21 approximates a straight line for $RH_c > \sim 95\%$ with a fit given by RH_c (%) = 68.9 + [2.77xRe (μm)]. The other passes are given similar fits. The two data points at 93% and 94 % are not included in the #21 fit indicating that most of the droplets have evaporated for those RH_c values. By using the linear fit relationship will cause the RH_c data to be underestimated for $RH_c < \sim 95\%$.
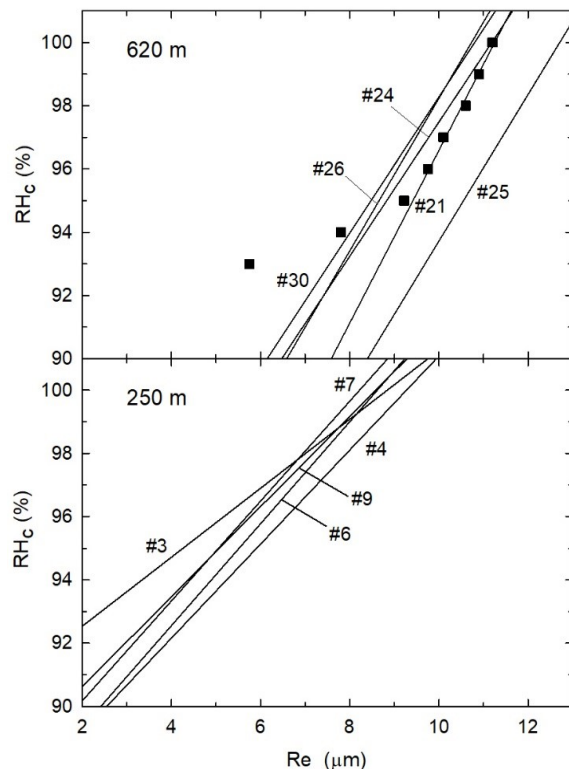

Fig. 4 – Relationship between RH_c in the entrained cloud-parcel mixture and the effective radius (Re) calculated from measured spectra exposed to RH_c as illustrated in Fig. 3 for pass #21. The squares data are for pass #21, and the other lines are approximate linear relationships for the passes (pass numbers listed in Gerber et al., 2008) at the two indicated levels above cloud base.

This simple approach of calculating the response of the measured droplet spectrum to sub-saturated conditions avoids mixing complexities shown in high-resolution modeling studies such as for DNS (e.g., Abma et al., 2013; Kumar et al., 2013) and for EMPM (Toelle and Krueger, 2014.) S transients and broadening of spectra during mixing described in the modeling are missing and thus cause uncertainties in the present approach.

4.2 Evaporation Time Dependence

The droplet growth equation is used to produce a record of the changing value of RH in the entrained parcel/cloud mixture as the droplets evaporate. Figure 5 shows RH as a function of time for pass #21 for a range of initial values of RH_c in the mixture. Curves for two values of N are shown with the solid curves for $\chi = 0.5$, and the dashed curves for $\chi = 1.0$. Curves approach the equilibrium values of RH exponentially. Most curves show a star indicating where RH has reached 99% of the equilibrium RH value where all droplets are assumed to

4

have evaporated. The increase in time for reaching equilibrium depends on the increase of the initial relative humidity RH_c given at TIME = 0 s. As initial RH_c approaches 100%, the TIME for equilibrium becomes very large. Curves with the same initial RH_c, but with larger value of N, increase RH_c more rapidly than those with smaller N, but they require more time to reach equilibrium. Kumar et al. (2013) shows similar transient behavior. The comparison of the curves in Fig. 5 with the 10-s time for τ_{mix} suggests that if initial RH_c values are low all droplets evaporate.
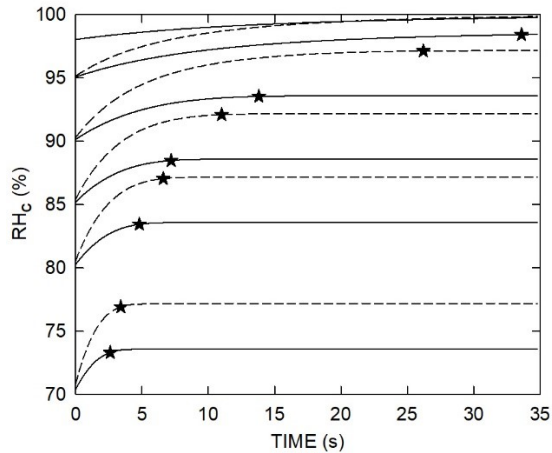

Fig. 5 – Change in relative humidity with time of the measured droplet spectrum for pass #21 as a function of the relative humidity RHc applied initially to the entrained parcel-cloud mixture for two values of the mixing fraction: $\chi = 0.5$ (solid curves), and $\chi = 1.0$ (dashed curves.) Stars indicate where 99% of the equilibrium value of RH is reached. Horizontal lines indicate total droplet evaporation.

A "reaction time scale" τ_{react} can be estimated from the curves in Fig. 5, where τ_{react} is the 1/e time for phase changes associated with droplet evaporation and restoration of an equilibrium vapor concentration (Lehmann et al., 2009.) The value of τ_{react} has a strong dependence on the initial value of RH_c. For example, τ_{react} ~ 2.5 s for RH_c = 80%, and τ_{react} ~ 20 s for RH_c = 98% in Fig. 5. The ratio of τ_{mix}/τ_{react} is defined by Lehman et al (2009) as the Damkoehler number (Da) which corresponds to homogeneous mixing following entrainment if Da << 1, and it corresponds to inhomogeneous mixing if Da >> 1, with Da = 1 separating the two conditions. Figure 5 shows that neither extreme Da values exist for Cu #21; however, Da <1 for RH_c > ~ 90%. The transition from inhomogeneous to homogeneous mixing also depends on the "transition length scale" defined by Lehmann et al. (2009) as $l^* = \varepsilon^{1/2} \tau_{react}^{3/2}$. The resulting mean value of l^* for #21 is ~2.4 m,

which means that entrainment scales smaller than this l^* should mix homogeneously and scales larger should mix inhomogeneously. The reduced Re parcels at the edges of the Cu #21 are smaller than l^* suggesting that homogeneous mixing is taking place.

5. PDF OF RH IN ENTRAINED PARCELS

The calculated straight-line relationships between Re and RH_c described in Section 4.1 can now be compared to each measured value of reduced Re described in Section 3. A match between the calculated and measured Re value gives an estimate of RH_c for the corresponding data point. The pdf histogram is generated in Fig. 6 that
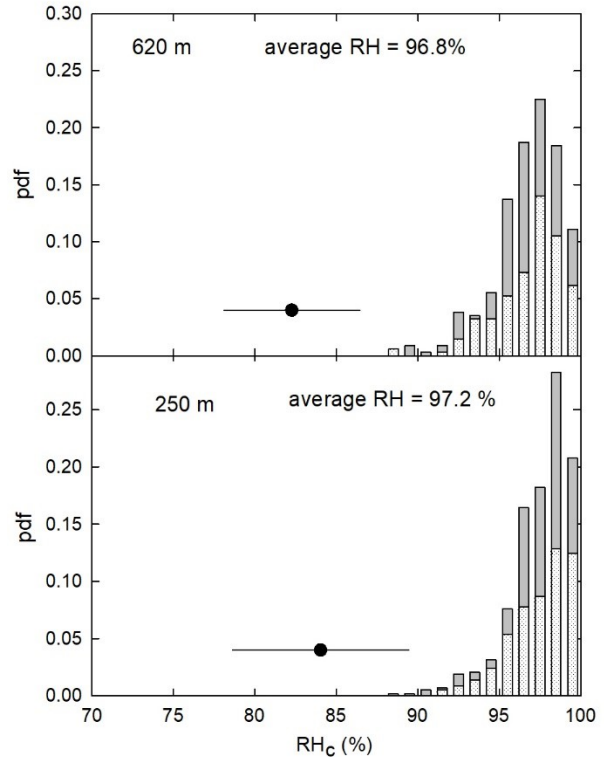

Fig. 6 – pdf of RH_c values resulting from matches between the measured and calculated values of Re (see text) for 5 passes at both levels above cloud base. Solid bars indicate rising cloudy air, and doted bars indicate descending cloudy air. Average RH_c values for the bars are listed. Solid data points indicate ambient relative humidity and its 2σ variability far from cloud edges.

represents the probability of RH_c in all data points with reduced Re in the 5 passes at the 620 m and 250 m levels. Also shown are the mean value of RH_c and the mean value of the ambient RH_e and its variability far from the Cu. The high values of RH_c in Fig. 6 correspond to the upper curves in Fig. 5 for which the times for total evaporation (stars data) are long, and τ_{react} are significantly larger than τ_{mix}. This means that the

associated mixing tends towards being homogeneous at as also previously suggested by Andrejczuk et al. (2006) for high RH values.

The pdf of RH_e rather than that of RH_c associated with the entrainment is ultimately the desired information. It can be estimated under isothermal and conservation of vapor mixing ratio (q) conditions by $q_{ve} = [q_{vm} - q_{vs}(1- \chi)]/\chi$ where the subscript e refers to the environment, m to the instantaneous mixture of entrained parcel and the cloud, and s to saturation. The shape of the RH_e histogram (not shown) is similar to that of RH_c, but the mean RH_e value is about 2% RH smaller.

There are uncertainties associated with Fig. 6, especially because of the lack of mixing history associated with this data. It is not known if evaporation is incomplete so that reduced values of Re should be smaller, or that the entrained mixture has aged so that reduced Re values should be larger. Values of the pdf for RH_c > 98% in Fig. 6 are too small given the noise in the measurements. Also, the noise in the data generates an uncertainty of about +/- 1% RH_c. Another uncertainty is the choice of one value (0.5) of χ used here. The value of χ likely has a wide range in Cu (e.g., see Toelle and Krueger, 2014) thus affecting the RH_c pdf histogram. Additional calculations show that RH_c shifts to larger values when χ > 0.5 and shifts to smaller values when χ < 0.5. The choice of parcel size also has an effect. Larger sizes would move the value of τ_{mix} closer to τ_{react}.

The RH_c values in Fig. 6 compare favorably with other estimates of RH_e associated with entrainment and obtained from observations in small Cu and using the mixing diagram approach. Small et al. (2013) finds a pdf range approximately between 90% and 99.5%, and Schmeissner et al. (2015) give a predominant range for RH_e of 90% to 99%.

6. DISCUSSION AND CONCLUSIONS

Reduced values of Re smaller than the approximately constant background values of Re are found in cloud parcels in RICO Cu showing that droplet evaporation is associated with entrainment. *The small sizes of the parcels are near the "transition length scale" suggesting that homogenous mixing is taking place.*

The present estimate of the average RH (relative humidity) associated with the entrainment-mixing process is 97%. This high value of sub-saturated RH suggests that the evaporation of the droplets is incomplete before the entrained mixture is homogenized with the rest of the Cu. The observed very rare presence of parcels with lengths as small as 20 cm within the cloud and with LWC = 0 g m^{-3} bears this out. *Again, homogeneous mixing appears to be active.* Other observations support the high values of RH: High RH values assumed to be associated with entrainment are found by Lu et al (2012) to be ~ 91% within 10 m-20 m of

cloud edge. The previously-mentioned mixing diagrams also suggest high RH values in the mixing process. Hues and Jonker (2008) and others describe moist descending shells surrounding Cu suggesting that the shells may be the source of high RH associated with entrainment.

What about the significant reductions in LWC without reductions in Re as often observed in the aircraft passes from the flight RF12? This looks very much like inhomogenous extreme mixing is taking place, as shown by Gerber et al. (2008), and concluded by a host of others in other Cu studies. This type of mixing produces data along a horizontal line in mixing diagrams. It is now proposed that this may not be the case. First, dilution of the cloud during entrainment by very high RH may cause the lack of Re reduction in the reduced LWC. Second, if inhomogenous extreme mixing is present, the resulting droplet evaporation should show some reductions in Re, because of the short time (2 ms) associated with the 500-Hz data rate of the PVM-100A probe in comparison to the longer droplet evaporation time even if RH_e is low. And third, the 20-cm resolution of the data has a resolution smaller by a factor of ~200 than the Kolmogrov scale (~ 1 mm) for these Cu where droplet evaporation occurs. Thus, reduced values of Re may be missed, especially if prior mixing has taken place.

It is concluded that homogeneous mixing is the dominant mixing behavior in these Cu. This conclusion applies only to the measurements made ~200 m below Cu top in growing RICO Cu from flight RF12. No analysis has been done with the high-rate data to see if such behavior exists at different heights in the Cu, or during different parts of the Cu life cycle as described by Katzwinkel et al. (2014.)

It is somewhat surprising that the mixing diagrams of Gerber et al. (2008) and those of Small et al. (2013) and Schmeissner et al. (2015) yield similar high values of RH associated with entrainment. The former is referenced to the observations at the level of each aircraft pass under the assumption that is where entrainment occurs. This is supported by Blyth (1993) who finds the source of entrained air not far above the pass, and by Hues et al. (2008) who finds the source just below and close to the pass. The latter two, including the seminal paper by Burnet and Brenguier (2007), references instead adiabatic LWC thought to be present at the source of entrainment. These mixing diagram differences are not large enough to prevent high RH results for both, because both mixing diagram approaches show the largest reductions in droplet size for small values of LWC for the former and low droplet concentration for the latter. The former approach gives less noisy and more consistent results for the mixing diagram with most passes showing relatively constant Re suggesting cloud dilution, showing decreased Re at small values of LWC suggesting evaporation near cloud edges, and showing

changes in Re and LWC without dilution suggesting the presence of secondary CCN activation.

This limited analysis dealt only with a small fraction of the high-resolution flight RF12 data; and there are more flights during RICO with such data. Still, this analysis leads to some questions and a recommendation: Does the present homogenous conclusion apply to other parts of the Cu such as the top of growing Cu, or in the wake of the Cu? Is high RH always associated with entrainment from the moist subsiding shell around Cu, or is the entrained air dry enough to limit secondary activation (Small et al., 2013)? Is the entrainment/detrainment, mixing behavior, and reductions in droplet sizes in the RICO trade-wind Cu specific to the dominant presence of hygroscopic sea-salt CCN? Half of the detrained air is re-entrained as suggested by Yeo and Romps (2013); does this relate to the stability of the droplet spectrum with height as observed by Gerber et al. (2008) in the RICO flight RF12? The CCN concentration below the inversion and between the Cu is approximately constant with height; how does this affect Cu microphysics? Why assume adiabatic LWC in estimating RH of the entrained air in mixing diagrams when measurements in small Cu show strongly reduced LWC not far above cloud base? Should the mixing diagram approach show independence of ambient RH (Pinsky and Khain, 2018)? Why does entrained air and mixing sometimes generate monomodal droplet size distribution, as in the present study, and sometimes bimodal and broadened distributions as shown by Lasher-Trapp et al. (2005) and Schmeissner et al. (2015)?

It would be desirable that modeling results for small Cu, such as those in trade-wind regimes, are related more frequently to the numerous existing observations in those Cu. This holds especially for high-resolution modeling for which including entrainment with secondary CCN activation in cloud containing typical droplet spectra would be desirable.

The best high-resolution microphysics data in Cu from the PVM probe are found in RICO and SCMS (Small Cumulus Microphysics Study) flights. While the PVM data resolution is still far from the Kologorov scale, most of this unique data (all archived by NCAR) has not been analyzed and should help further our understanding of the entrainment and mixing process in small Cu.

7. REFERENCES

Abma, D., T. Heus, and J.P. Mellado, 2013: Direct numerical simulation of evaporative cooling at the lateral boundary layer of shallow cumulus clouds. *J. Atmos. Sci.,* 70, 2088-2102, doi:10.1175/JAS-d-12-0230.1.

Andrejczuk, M., W.W. Grabowski, S.P. Malinowski, and P.K. Smolarkiewicz, 2006: Numerical simulation of cloud-clear air interfacial mixing: Effects of cloud microphysics. *J. Atmos. Sci.*, 63, 3204-3225.

Baker, M.B., and J. Latham, 1979: The evolution of droplet spectra and the rate of production of embryonic raindrops in small cumulus clouds. *J. Atmos. Sci.*, 36, 1612-1615.

_____, R.G. Corbin, and J. Latham, 1980: The influence of entrainment on the evolution of cloud droplet spectra. I: A model of inhomogeneous mixing. *Quart J. Roy. Meteor. Soc.*, 106, 581-598, doi:10.1002/qj.49710644914.

_____, R.E. Breidenthal, T.W. Choularton, and J. Latham, 1984: The effects of turbulent mixing in clouds. *J. Atmos. Sci.*, 41, 299-304.

Beals, M.J. and others, 2015: Holographic measurements of inhomogenous cloud mixing at the centimeter scale. *Science, 350*, 87-90.

Blyth, A.M., 1993: Entrainment in cumulus clouds. *J. Appl. Meteorol.*, 32, 626-641.

_____, and J. Latham, 1991: A climatological parameterization of cumulus clouds. *J. Atmos. Sci.*, 48, 2367-2371.

Burnet, F., and J.-L. Brenguier, 2007: Observational study of the entrainment-mixing process in warm convective clouds. *J. Atmos. Sci.*, 64, 1995-2011, doi:10.1175/JAS3928.1.

Damiani, R., G. Vali, and S. Haimov, 2006: The structure of thermal in cumulus from airborne dual-Doppler radar observations. *J. Atmos. Sci.*, 63,1432-1450.

Gerber, H., B.G. Arends, and A.K. Ackermann, 1994: New microphysics sensor for aircraft use. *Atmos. Res.*, 31, 235- 252.

_____, G.M. Frick, J.B. Jensen, and J.G. Hudson, 2008: Entrainment, mixing, and microphysics in trade-wind cumulus. *J. Meteor. Soc. Japan,* 86A, 87-106, doi:10.2151/jmsj.86A.87.

Hues, T., and H.J.J. Jonker, 2008: Subsiding shells around shallow cumulus clouds. *J. Atmos. Sci.*, 65, 1003-1018.

_____, G. Van Dijk, H.J.J. Jonker, and H.E.A. Van Den Akker, 2008: Mixing in shallow cumulus clouds by Lagrangian particle tracking. *J. Atmos. Sci.*, 65, 2581-2597.

Jarecka, D., W.W. Grabowski, H. Morrison, and H. Pawlowska, 2013: Homogeneity of the sub-grid-scale turbulent mixing in large-eddy simulation of shallow convection. *J. Atmos. Sci.*, 70, 2751-2767, doi:10.1175/JAS-D-13-042.1.

Jensen, J.B., and M.B. Baker, 1989: A simple model of droplet spectral evolution during turbulent mixing. *J. Atmos. Sci*., 46, 2812-2829.

Katzwinkel, J., H. Siebert, T. Heus, and R.A. Shaw, 2014: Measurements of turbulent mixing and subsiding shells in trade wind cumuli. *J. Atmos. Sci*., 71, 2810-2822, doi:10.1175/JAS-D-13-0222.1.

Kumar, B., J. Schumacher, and R.A. Shaw, 2013: Cloud microphysical effects of turbulent mixing. *Theor. Comput. Fluid Dyn*., 27, 361-376, doi:10.1007/s00162-012-0272-z.

Lasher-Trapp, S.G., W.A. Cooper, and A.M. Blyth, 2005: Broadening of droplet size distributions from entrainment and mixing in a cumulus cloud. Quart. *J. Roy. Meteor. Soc*., 131, 195-220.

Lehmann, K., H. Siebert, and R.A. Shaw, 2009: Homogeneous and inhomogeneous mixing in cumulus clouds: Dependence on local turbulence structure. *J. Atmos. Sci*., 66, 3641-3659, doi:10.1175/2009JAS3012.1.

Lu, C., Y. Liu, S. Niu, and M. Vogelman, 2012: Lateral entrainment rate in shallow cumuli: Dependence on dry air sources and probability density functions. *Geophys. Res. Lett*., 39, L20812, doi:10.1029/2012GL053646.

Pinsky, M., and A. Khain, 2018: Theoretical analysis of mixing in liquid clouds – Part IV: DSD evolution and mixing diagrams. *Atmos. Chem. Phys*., 18, 3659-3676, Https://doi.org/10.5194/acp-18-3659-2018.

Rauber, R.M., B. Stevens, and co-authors, 2007: Rain in shallow cumulus over the ocean- The RICO campaign. *Bull. Amer. Meteor. Soc.,* 88, 1912-1928.

Schmeissner, T., R.A. Shaw, J. Ditas, F. Stratman, M. Wendisch, and H. Siebert, 2015, *J. Atmos. Sci*., 72, 1447-1464, doi:10.1175/JAS-D-14-0230.1.

Small, J.D., P.Y. Chuang, and H.H. Haflidi, 2013: Microphysical imprint of entrainment in warm cumulus. *Tellus B 2013*, 65, 19922, http://dx.doi.org/10.3402/tellusb.v65i0.19922.

Toelle, M.H., and S.K. Krueger, 2014: Effect of entrainment and mixing on droplet size distributions in warm cumulus clouds. *J. Adv. Model. Earth Syst*., 6, doi:10.1002/2012MS000209.

Yeo, K., and D.M. Romps, 2013: Measurement of convective entrainment using Lagrangian particles. *J. Atmos. Sci., 70,* 266-277.